SCALING PERFORMANCE ANALYSES WITHIN BI-PROPELLANT SYSTEMS USING ESPSS

Jorge Ruiz-Torralba [(1)], Bayrem Zitouni [(1)], Markus Peukert [(1)], Ingolf Fischer [(1)]

[(1)] OHB System AG, Universitätsallee 27-29, 28359 Bremen, Email: jorge.ruiz@ohb.de

Abstract

This paper outlines the transient phenomena experienced in bi-propellant propulsion systems at multiple scales. ExoMars 2016 propulsion system is set as reference case of validation on ESPSS. According to this validation, the propulsion system is scaled up to study the transient implications over the feeding system. This study is used to define OHB propulsion guidelines for future missions (i.e. moon landers), in which more powerful propulsion systems will play a main role.

The Propellant Isolation Assembly (PIA) of the Engineering Validation Model (EVM) test bench is the subject under analysis. OHB System AG conducted extensive priming and water hammer tests using MON-1 and MMH as live propellants. These models are updated to the latest version of ESPSS (v3.4.0), considering numerical, fluid-dynamic and physical modelling updates and in-house developments. Priming and water hammer cases are simulated on ESPSS and validated against experimental data. Afterwards, this propulsion system is scaled up to greater mass flows at both MON and MMH branches.

As result, OHB design guidelines for powerful bi-propellant systems are drawn using ESPSS. Furthermore, the advantages and limitations of ESPSS to reproduce transient phenomena in complex fluidic networks are studied (applied to MON and MMH propellants). The conclusions highlighted in this paper can be used as potential reference to define future ESPSS developments.

1 Introduction

The propulsion system of ExoMars 2016 is used as application case due to the extensive test data available at OHB System AG [1]. This propulsion system is a bi-propellant pressure regulated system, which uses MON-1 and MMH as live propellants and He as pressurant (see Figure 1). The system is equipped with one Main Engine (ME) of 400N thrust and 20 Reaction Control Thrusters (RCTs) of 10N thrust (10 thrusters are nominal and the other 10 thrusters are redundant). In this paper, the section under analysis is the Propellant Isolation Assembly (PIA), which goes from the tanks outlet up to the thrusters' inlet.

The priming and water-hammer phenomena within PIA are studied using the European Space Propulsion System Simulation (ESPSS). The models are validated on the latest version of ESPSS (v3.4.0). Physical-numerical issues are encountered on ESPSS as part of the validation process, requiring to carry out in-house developments to solve them. Such developments enable to obtain a proper balance in terms of physical reproduction and CPU ti-

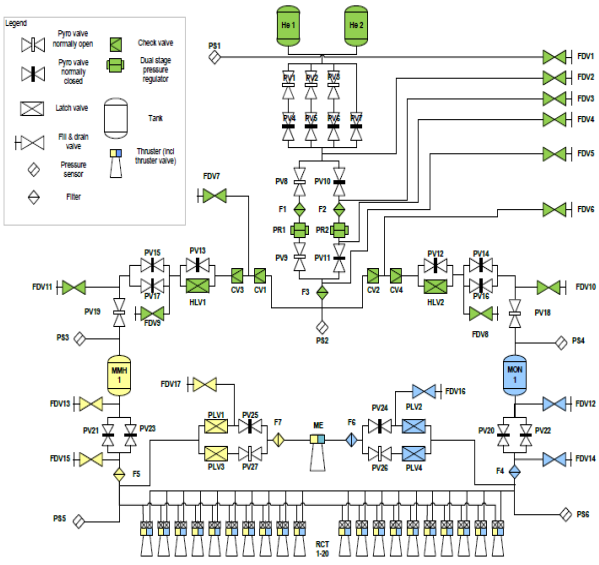

Figure 1: ExoMars 2016 Propulsion Schematic

me. Based on the validation outcomes, the propulsion models are scaled up as function of the mass flow, the tanks pressure, the piping diameter and the piping lengths. The influence of these design drivers over the pressure peaks of the feeding system is studied.

The aim of this paper is to establish scaling rules applied to the pressure peaks experienced during the priming and water hammer, in order to guide the design of more powerful bi-propellant systems. Such scaling rules depend on multiple physical phenomena and geometrical features, for what ESPSS offers optimum capabilities in terms of modelling flexibility and physical reproduction for systems design analyses. In this paper, the scaling rules are applied to MON/MMH bi-propellant systems, but this methodology is easily expandable to other propellants thanks to the modelling flexibility of ESPSS (i.e. analyses of bi-propellant systems using green propellants). In addition, these scaling up studies are applicable for the use of more powerful thrusters and/or for the increase of the number of thrusters. Therefore, ESPSS provides multiple benefits for these study cases, since it enables to simulate complex physical phenomena by means of graphical and easily reconfigurable simulations.

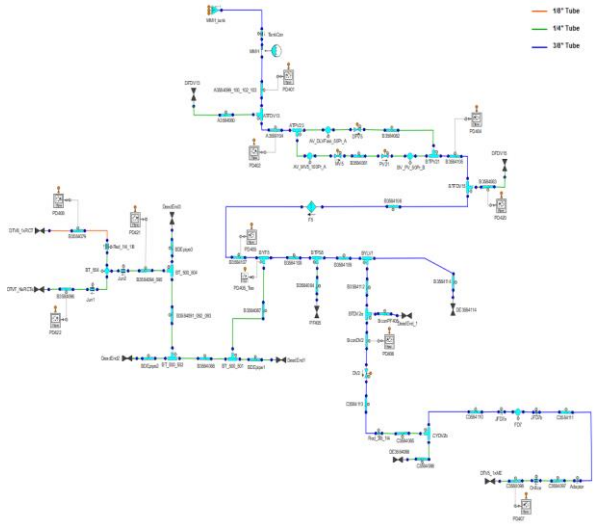

Figure 2: ESPSS schematic for MMH PIA

2 Validation on ESPSS v3.4.0

The propulsion system of ExoMars 2016 was validated on ESPSS v2.4.0 [1]. In the former validation activities, two main issues were encountered by OHB during transient simulations:

- Physical discontinuities in the thermodynamic state determination of MON and MMH. Non-physical pressure peaks were obtained in the priming simulations, as it is shown by the default ESPSS in Figure 4.
- Long CPU times for the priming simulation of both MON and MMH branches, as it is illustrated in Figure 5 and Figure 6 for ESPSS v2.4.0.

These validation models are updated to the latest ESPSS (v3.4.0) to take advantage of the physical and numerical improvements included in the simulation platform. To improve the CPU time, CVODE SPARSE is applied as numerical solver. This solver shows the best numerical performance on ESPSS. In addition, in-house developments are carried out to solve the physical discontinuities.

The discontinuities in the thermodynamic state determination are induced by the use of the real fluid formulation of MON and MMH. The perfect liquid formulation does not show such discontinuities; however, the thermodynamic database applied with this methodology is quite scarce for the priming phenomenon. Furthermore, the priming pressure peaks are underestimated with perfect liquid formulation in comparison with real fluid formulation. Figure 3 shows the pressure drop induced in the pyro-valve upstream the ME, which is two orders of magnitude greater with perfect liquid formulation. It results in a smaller pressure peak at the ME inlet and the subsequent pressure peak underestimation.

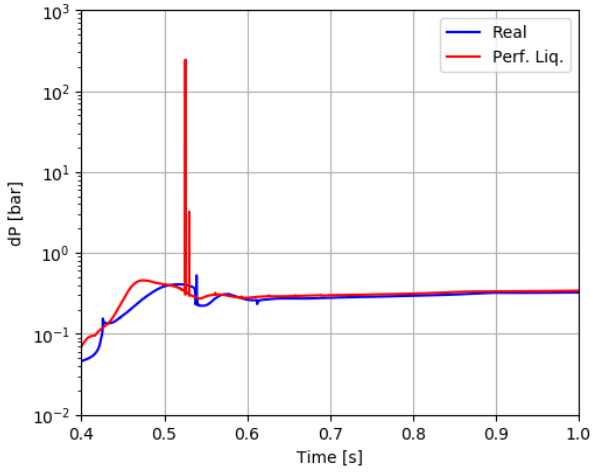

Figure 3: Pressure drop induced in the pyro-valve upstream of the ME at MON branch

Once the perfect liquid formulation is disregarded due to the pressure drop imposed in the pyro-valve, the real fluid formulation is selected as way-forward. Nonetheless, this formulation shows relevant physical discontinuities during the priming process, as Figure 4 illustrates with the pressure evolution given by the default ESPSS. The reasons of these discontinuities are numerically and physically coupled due to the reduced number of thermodynamic points available at the ESPSS fluid properties database of MON and MMH. In particular, the reduced number of points at low pressures. In-house developments

in the source code of the ESPSS were done by OHB to attenuate these numerical-physical discontinuities, as it is shown in Figure 4.

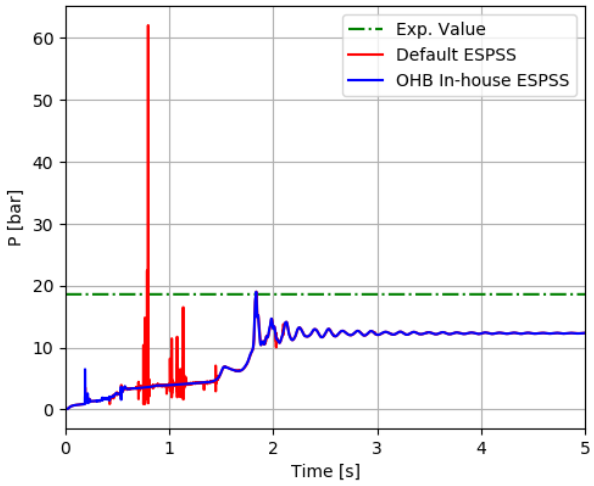

Figure 4: Pressure evolution along priming simulation at an intermediate PT.

Indeed, these developments also improve the CPU time and enable to simulate the system at even lower vacuum pressure (not crashing the simulation as it can occur with the default ESPSS).

Applying the aforementioned upgrades, the validation outcomes shown in Figure 5 and Figure 6 are obtained. The improvement in the relative error of the pressure peaks and in the CPU time is remarkable. In addition, all validation outcomes are conservative with ESPSS v3.4.0, as the sign (+) illustrates in both summary reports. The values in green colour represent the maximum pressure peak in absolute terms. Note that these values show the lowest relative error among all sensors per branch and simulation case. So the validation is quite successful applied to the foremost pressure surges. Nonetheless, the relative error at RCT for MON priming is relevant. At this location, the model does not reproduce properly the pressure waves' reflections at highly-transient two-phase flows. In spite of it, the two main goals of the validation (improving the relative error of the physical phenomena and reducing the CPU time) are fulfilled with the new validation using ESPSS v3.4.0.

Figure 5: Priming validation outcomes

Branch	Location	Rel. Err. (%) [v2.4.0]	Rel. Err. (%) [v3.4.0]	CPU time [v2.4.0]	CPU time [v3.4.0]
MON	ME	-29.0	+1.5	125 h	14 min
	5 RCTs	-38.0	+3.1		
	RCT	+13.0	+86.6		
MMH	5 RCTs	+20.0	+19.1	23 h	8 min
	RCT	-3.0	+3.0		

Figure 6: Water-hammer validation outcomes

Branch	Location	Rel. Err. (%) [v2.4.0]	Rel. Err. (%) [v3.4.0]	CPU time [v2.4.0]	CPU time [v3.4.0]
MON	ME	-25.0	+2.0	48 min	32 s
	5 RCTs	-7.0	+8.0		
	RCT	+32.0	+9.0		
MMH	ME	-20.0	+4.0	30 min	20 s
	5 RCTs	+9.0	+11.0		
	RCT	+8.0	+10.0		

3 Model scaling-up for greater mass flows

According to the validation outcomes described in the former section, the models are scaled up to greater mass flows in order to study the pressure peaks during priming and water hammer.

3.1 Priming cases

For priming cases, the mass flow is scaled up by means of increasing the tanks pressure, the piping diameters and the piping lengths. The reference results to establish the pressure peak factor are taken from the baseline results of ExoMars 2016. They correspond to a factor of increase of 1 in both X and Y axes (i.e. Factor of Pressure Increase = 1 and Factor of Pressure Peak Increase = 1 in Figure 7).

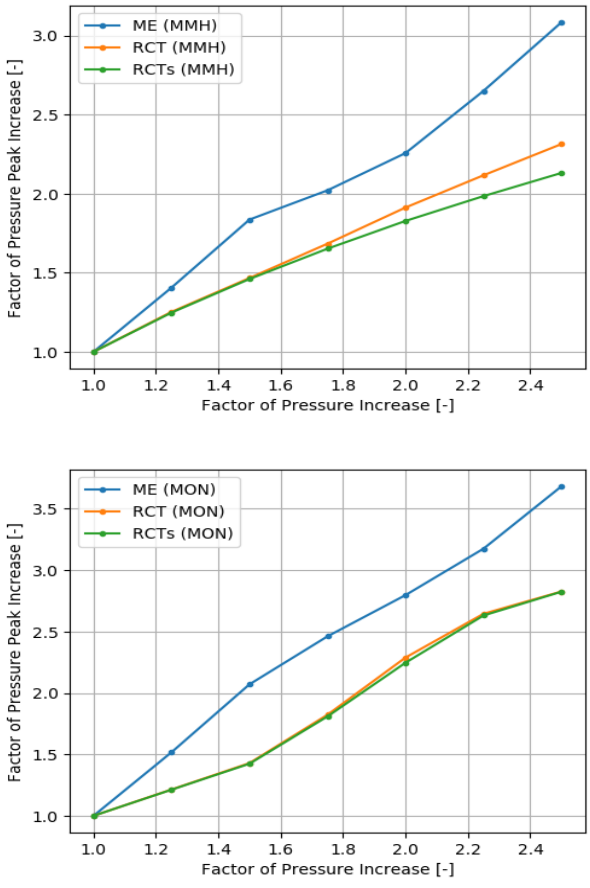

Figure 7: Priming peaks based on tanks pressure

The most influential parameter over the priming peaks is the tank pressure, as it is shown in Figure 7. The peaks increase linearly with the tank pressure, since the mass flow scales linearly with the pressure for the same piping geometry and vacuum pressure in the feeding lines. For the same range of pressure increase factor, MON branch provides a greater factor of increase.

The original piping diameter has been increased in the different branches of the feeding system (being all diameters increased at the same time). This parametric analysis increases the original diameter to the next diameter available in the market (i.e. in the first increase case, 1/4" pipes are increased to 3/8" pipes and, in the second increase case, 1/4" pipes are increased to 1/2" pipes).

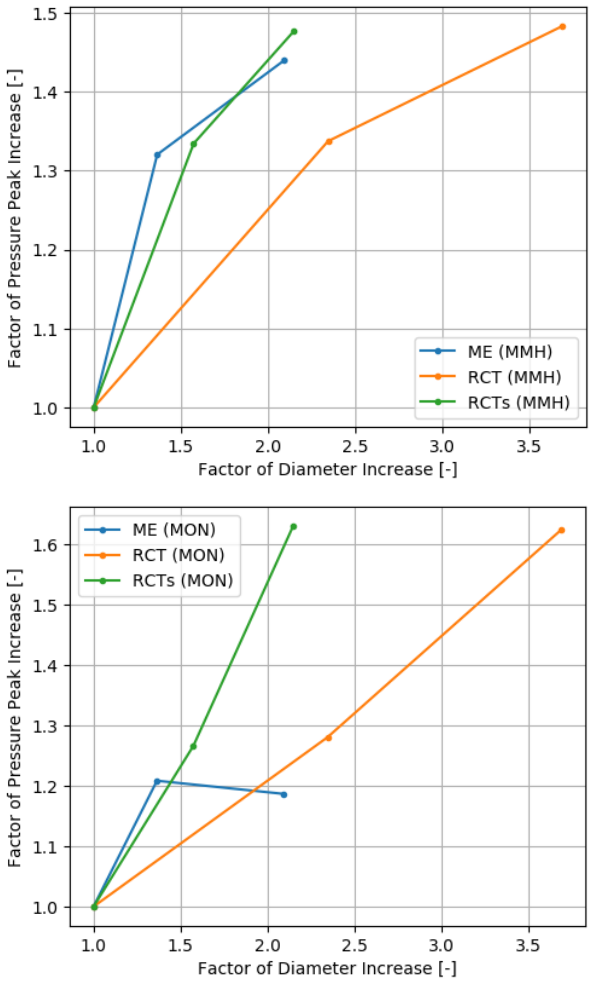

Figure 8: Priming peaks based on piping diameter

In this way, Figure 8 shall be read as a succession of cases, where the first point is the baseline model without any increase, the second point shows the first increase case and the last point shows the second increase case. For that, the factor of diameter increase is not the same in all sensors locations (originally ME pipeline is 3/8", RCTs is 1/4" and RCT is 1/8").

For MMH case, all pressure peaks increase with the diameter. Under the same vacuum pressure conditions and tank pressure, the mass flow is increased with the piping diameter and the friction losses are reduced. The reduction of the pressure peak slope in the last case of MMH is induced by the cushioning effect of having a greater amount of non-condensable gas in the feeding pipes. For MON case, the pressure peaks are also increased from the baseline case to the first diameter increase case. Nonetheless, the pressure peak is decreased in the ME at the last case. This decrease is triggered by the cushioning effect of the non-condensable gas within this line, which is the longest piping line of the feeding system. Thus, increasing its diameter has an important effect on the amount of non-condensable gas. As consequence of the mentioned pressure peak drop at the ME branch, greater mass flows and pressure peaks are experienced in the rest of branches, as the greater positive slope at RCT and RCTs show in Figure 8.

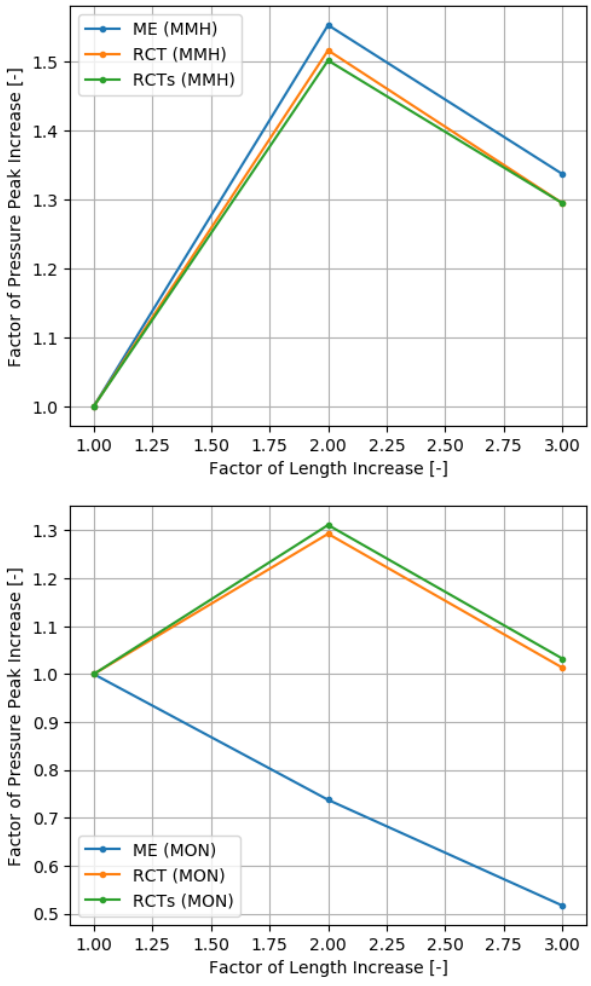

Figure 9: Priming peaks based on piping length

The original piping length of the whole system is increased as a whole in this analysis, as it is shown in Figure 9, where all locations show the same length increase factor. In MMH case, the length increase factor of 2 leads to greater pressure peaks since the fluid has a longer path to accelerate. In other words, the impact velocity of the liquid column is greater. On the other hand, the length increase factor of 3 shows an attenuation of the pressure peak due to the greater cushioning effect of the non-condensable gas, which counterbalances the longer acceleration path. Regarding RCT and RCTs sections, the first length increment triggers a greater pressure surge; meanwhile, the pressure surge drops for a length increase factor of 3 as consequence of the damping effect caused by the non-condensable gas. In MON case, the increase of the piping length decreases the priming pressure peak at the ME because of the larger cushioning effect of the non-condensable within the longest piping section of the feeding system. For RCT and RCTs sections, an analogous trend to MMH is followed. The first increment does increase the pressure surge, but the last one is attenuated by the non-condensable gas damping.

Therefore, the priming pressure peaks are mainly governed by the tank pressure under the same piping vacuum conditions. The increase of the piping diameter and length also increases the pressure peak, but with lower influence. It is worth pointing out that the diameter and length increase depends on the particular geometrical features of the feeding system. Their increase could also decrease the pressure peaks due to the cushioning effect of the non-condensable gas.

3.2 Water hammer cases

For water hammer cases, the demanded mass flow per thruster is increased. For each of these mass flows, the influence of the tank pressure and the piping geometry over the induced water hammer on other thrusters is analysed. Due to the length constraints of this paper, only the water hammer case of the MON branch is described (worst-case scenario due to the greatest mass flow at the ME inlet).

The mass flow required by the 400N thruster (ME) is considerably greater than the one demanded by the 10N RCTs. Consequently, the water hammer triggered by the shut-off of this engine represents the worst-case scenario for the induced water hammer at the inlet of the closest RCT (although the piping length between ME and the closest RCT is significantly larger in comparison with nearby RCTs). The mass flow through the ME is scaled up to reproduce the operation of several MEs, as it would be required in more powerful bi-propellant systems with a cluster of MEs (i.e. moon lander).

The tank pressure is not influential over the self-induced water-hammer at ME. This pressure peak scales with the mass flow through the main engine, as it is illustrated in Figure 10. Regarding the induced pressure peak over the RCT, the tank pressure only shows a limited influence at high pressure increments. However, this range of tank pressures increase will not be feasible due to priming peaks constraints or pressure safety limitation at launch.

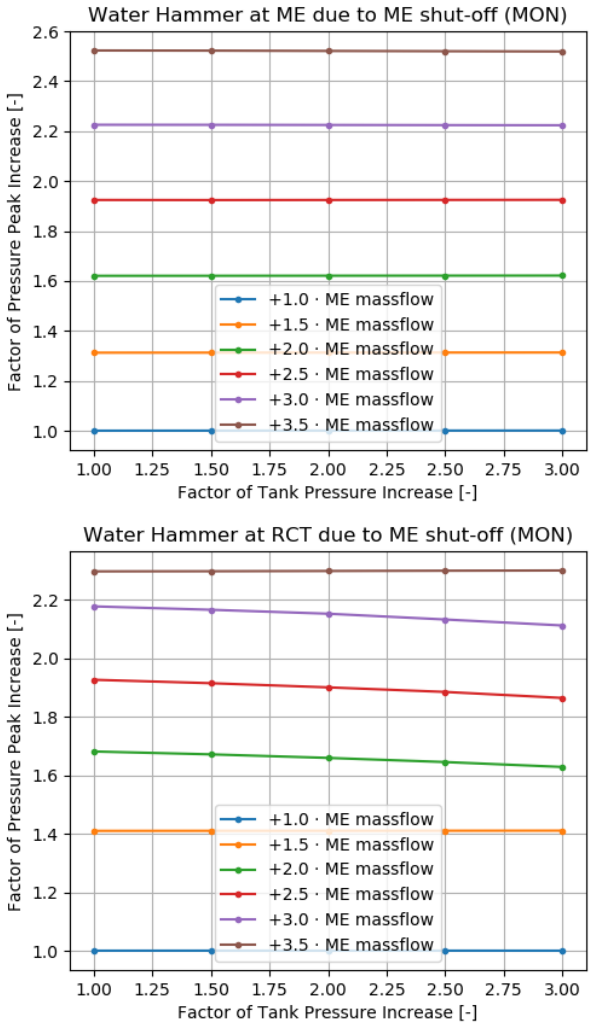

Figure 10: Water-hammer peaks based on tanks pressure

As it is shown in Figure 11, the pressure peaks at ME scales with the mass flow injected at the thrusters inlet. For a given mass flow and tank pressure, the increase of the diameter leads to a decrease of the fluid velocity at the inlet. Consequently, the velocity variation due to the inlet valve closing is smaller and, analogously, the pressure peak. A similar tendency is shown by the pressure peak at RCT, but attenuated due to pressure losses suffered by fluid along the trip from ME up to RCT.

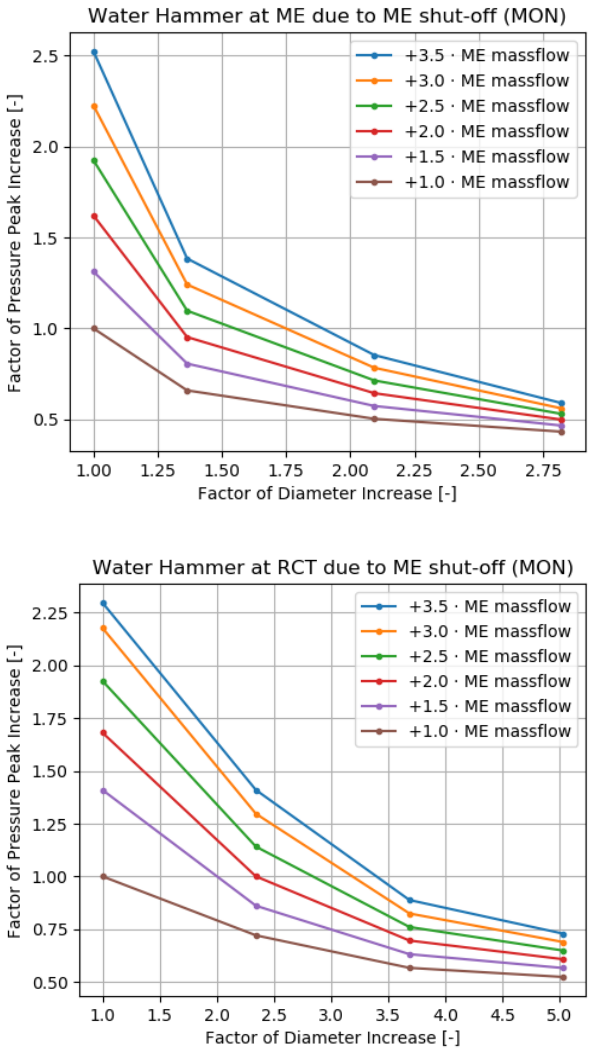

Figure 11: Water-hammer peaks based on piping diameters

Figure 12 shows the influence of the piping length over the water-hammer pressure peaks. The pressure peak increases with the mass flow through the main engine again. In addition, the pressure peak at ME increases with the piping length since inertia of the flow along the pipe is greater. In other words, when the valve is closed, the adiabatic compression of the fluid is longer because the compressed fluid needs more time to start the reverse flow motion.

The pressure peak at RCT is determined by the combination of the pressure peak magnitude at ME and the pressure losses experienced by the reverse flow along the piping. The greater length increases the pressure peaks at ME. The longer piping leads to greater friction losses that damp the pressure peak at RCT. Besides, the increase of the pressure peaks leads to a greater fluid velocity, scaling the friction losses as v^2. In this way, the cases of 1.5x and 2xME mass flow shown in Figure 12 show a drop in the pressure peak of RCT for a length factor of 1.5. In these cases, the pressure peak induced by the greater mass flow is not enough to counterbalance the greater friction losses from ME to RCT. Once the ME mass flow is greater than 2x ME mass flow, the pressure peak at ME governs over the pressure losses, leading to greater pressure peaks at RCT.

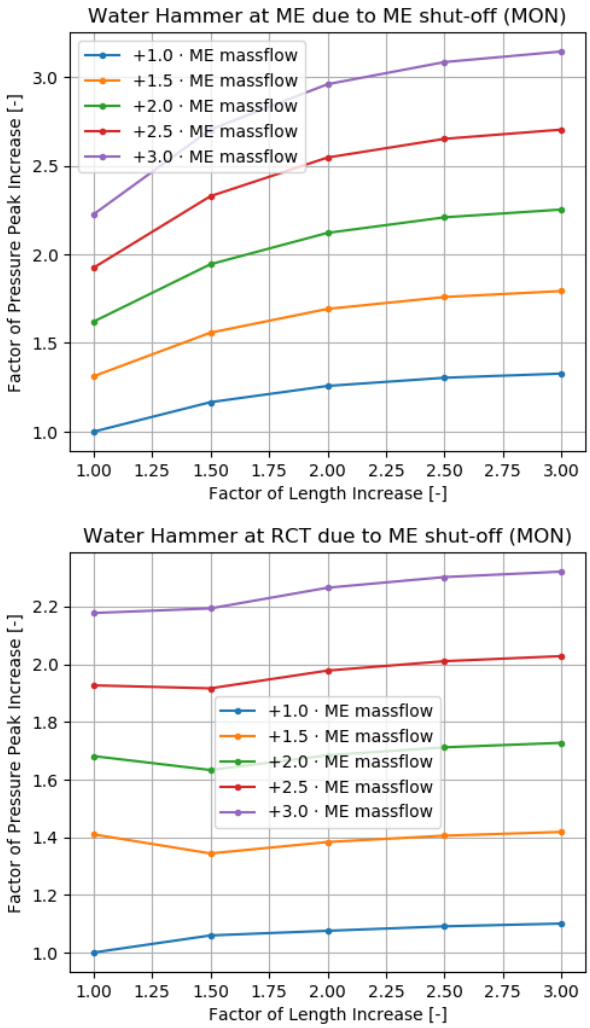

Figure 12: Water-hammer peaks based on piping length

Therefore, the water-hammer pressure peaks scale up with mass flow injected and length of the piping upstream of the ME. For a given mass flow, the pressure peaks significantly decrease with the piping diameter. Lastly, they are almost independent of the tank pressure.

4 Conclusions

The main conclusions that can be drawn are the following. ExoMars 2016 models have been updated to the latest version of ESPSS (v3.4.0). This update has solved the main issues found in the former validation activities (using ESPSS v2.4.0). First, the simulation agreement with the experimental results is improved. The relative errors of the validation

have been reduced, especially in the greatest pressure peak per propellant branch (as it is shown by the green values in Figure 5 and Figure 6). Note that the maximum deviation is +4% for the greatest pressure peaks among all cases. Second, the CPU time of all models have been significantly reduced, passing from hours of simulation to a few minutes (see Figure 5 and Figure 6).

In addition, OHB design guidelines for more powerful bi-propellant systems are drawn using ESPSS. These analyses have addressed the influence of the main design drivers affecting the pressure peaks during both priming and water-hammer phenomena. On the one hand, priming pressure peaks are mainly governed by the tank pressure. Scaling up the piping geometry also increases the priming peaks as a general rule, although it might damp the pressure peaks for long pipes due to the cushioning effect of non-condensable gas. On the other hand, water-hammer pressure peaks scale up with the thrusters' mass flow. For a demanded mass flow by thrusters at steady state, increasing the piping diameter reduces the induced pressure peaks; whereas, increasing the piping length increases these pressure peaks. The combination of these tendencies are used to determine the design guidelines for more powerful systems. It is worth pointing out that this paper scales the pressure peaks in quantitative terms, adding a relevant added value supported by physical modelling. Lastly, the scale up process shown herein can be applied for the use of more powerful thrusters and/or for the use of a greater number of thrusters.

These design guidelines are aligned with OHB propulsion strategy for more powerful systems, such as moon landers. Combining sloshing analyses on the propellant tanks (and their influence on EL3 GNC), multi-thruster plume iterations [2] and plume iterations with lunar surface (as an internal development program).

Unfortunately, ESPSS shows certain modelling limitations that should be improved as part of the continuous development of the tool. The main drawbacks identified as part of these activities are:

- The default ESPSS shows numerical discontinuities in the thermodynamic state determination during the priming of MON and MMH (see Figure 4). These discontinuities combine numerical and physical aspects, which shall be solved. A potential solution for this numerical-physical issue is discovered by OHB and it is proposed as a way-forward (it cannot be disclosed in this paper).
- The thermodynamic database of MON and MMH on ESPSS does not include enough thermodynamic state points at low pressures. The lack of thermodynamic state points in this region is the source of the reaming physical discontinuities seen in Figure 4 for OHB in-house ESPSS.
- Improvement of junctions/valves modelling during highly-transient two-phase flows. Figure 3 shows a case where a non-physical pressure drop is imposed, leading to an artificial-numerical damping of the priming pressure peaks by means of perfect liquid formulation. The non-proper determination of the pressure drop at junctions can be also extrapolated to tees under highly-transient two-phase flows. Notice that a +86.6% of relative error is obtained at RCT pressure sensor for MON priming (see Figure 5).

In spite of the aforementioned limitations of ESPSS, it is worth pointing out the outstanding capabilities offered by the tool. This tool is able to assist the design of very complex feeding systems by means of modelling highly-transient physical phenomena. It also provides quite competitive CPU times, being able to simulate complex fluidic networks in a few minutes. Finally, the modelling flexibility given by the non-casual coding and the graphical object oriented approach enables to carry out multiple parametric analyses that highly support the design decision process of propulsion systems.

5 References

[1] V. Tregubow, "Fluid transient simulation for the ExoMars bi-propellant propulsion subsystem," in *European Space Propulsion Conference 2014*, Cologne, 2014.

[2] R. Kast, "Multi-thruster Plume Interaction: New Modelling Approach," in *Space Propulsion Conference 2022*, Estoril, 2022.